Proceedings of the ASME 2009 International Design Engineering Technical Conferences & Computers and Information in Engineering Conference
IDETC/CIE 2009
August 30 - September 2, 2009, San Diego, California, USA

DETC2009-87844

A MODAL APPROACH FOR CHAOTIC VIBRATIONS OF A DRILLSTRING

Kathira Mongkolcheep
Department of Mechanical Engineering
Texas A&M University, College Station, Texas 77845, U.S.A.

Alan Palazzolo
Department of Mechanical Engineering
Texas A&M University, College Station, Texas 77845, U.S.A.

Annie Ruimi
Department of Mechanical Engineering
Texas A&M University at Qatar, Doha, Qatar

Randall Tucker
Department of Mechanical Engineering
Texas A&M University, College Station, Texas 77845, U.S.A.

ABSTRACT
The purpose of this paper is to present a methodology to predict vibrations of drilllstrings for oil recovery service. The paper extends a previous model in the literature to include drill collar flexibility utilizing a modal coordinate condensed, finite element approach. The nonlinear effects of drillstring / borehole contact, friction and quadratic damping are included. Bifurcation diagrams are presented to illustrate the effects of speed, friction, stabilizer gap and drill collar length on chaotic vibration response. A study is conducted on factors for improving the accuracy of Lyapunov Exponents to predict the presence of chaos. This study considers the length of time to steady state, the number and duration of linearization sub-intervals, the presence of rigid body modes and the number of finite elements and modal coordinates. The results may be helpful for computing Lyapunov exponents of other types of nonlinear vibrating systems with many degrees of freedom.

1 INTRODUCTION
High demand for energy has forced the oil and gas industry to seek improved drilling methods. Their goal is to prevent or reduce failures in order to reduce cost and air pollution by eliminating equipment replacement, repeated drilling of wells and unnecessary down time. Failures are quite often associated with severe vibrations of the lower part of the drillstring (DS) due to the interaction between the rotating drillstring and the rock formation or surrounding water and drilling mud.

Typically, a drillstring is composed of a hoisting and turning mechanisms (draw work, kelly or top drive), a drillpipe, drill collars, stabilizers and a drill bit or rock cutting tool. Drill collars are thick-walled, large diameter pipes which provide the weight on bit (WOB) and prevent drill pipes from buckling by keeping them in tension at the surface. Stabilizers (centralizers) are located along the drill collars and above the drill bit, in the lower part of the DS known as the bottom hole assembly (BHA). The stabilizers have short sections and a diameter near that of the borehole (or wellbore) to help to center the BHA. They also improve the drill bit performance by preventing bending of the lower part of the drill collar [1, 2]. Figure 1 depicts a truncated length of drillpipe (top**),** a string of drill collars with 2 end stabilizers, the BHA and the drill bit. Interactions of the DS and the drilling fluid (mud), contact forces between the wellbore and drillstring and interaction between the borehole and the drill bit may cause severe vibrations that can damage the drilling equipment, the drillstring and/or the stabilizers.

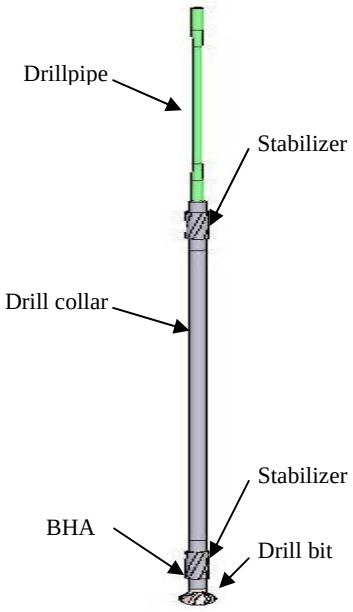

Figure 1. Major Components of the Drillstring Model.

Three types of vibrations are predominant in drilling. Axial vibrations (AV) results from interactions between the bits and the hole bottom. This may result in large fluctuations of WOB and suspended particulate phase SPP, erratic rate of penetration ROP, shaking of surface equipment at shallow drilling depths, loss of tool face and poor directional control. Torsional vibration (TV) results from drill collar resonance, bit chatter, stick-slip (SS) interaction between the bit and formation and modal coupling. Severe SS motion may even cause a stopping or reversing of the bit direction. Lateral vibrations (LV) are called whirling motion and results from interactions between the bits and formation, mass imbalance, bit whirl, and from fluid forces around the drillstring. LV also results from coupling between the lateral and axial directions and the presence of axial bit-bounce motions.
The DS can vibrate in any or all of these types of vibrations and experience failures as indicated by reduction in the rate of penetration and drillstring or bit damage.

This paper focuses on predicting lateral chaotic vibrations that result from imbalance, stabilizer borehole impacts and friction, and nonlinear damping. A lateral degree of freedom is assumed at the bit. This is a reasonable assumption because of oversize cutting (bit walk, runout, and formation swell compensation) which leaves a clearance between the bit-through diameter and the as drilled gage hole. A Timoshenko beam based finite element code is employed to model the drillpipe and the drill collars between two stabilizers. Modal condensation is utilized to reduce the number of degrees of freedom and computational time. The vibration response is categorized by the use of nonlinear dynamics techniques which include Lyapunov exponents (LE), bifurcation diagrams and Poincare maps. LE's provide a measure of divergence or convergence of nearby trajectories and are calculated from the modal coordinate responses as an indication of chaotic vs. non-chaotic behavior. Chaotic motion must produce at least one positive Lyapunov exponent, hence it is sufficient to determine only the maximum LE.

The proposed model includes mass eccentricity, fluid damping, Coulomb friction and stress stiffening due to the axial load from the drill collar weight.

Vibration response predictions may assist drilling rig operators in changing a variety of controlled parameters such as rotary speed, drilling mud composition, stabilizer gaps, drill collar length, etc. This will ultimately lead to improved procedures for oil and gas recovery, a decrease in equipment failure, cost savings and reduced emissions.

2 LITERATURE REVIEW

Most of the drillstring vibration literature focuses on models of parts or components of the entire drilling rig. Boundary conditions are assumed to facilitate these partial system models. These models are utilized to help explain direct, or indirect (damage) measurements of drillstring vibration.

Lin et al. [3] proposed a single-degree-of-freedom torsional model including the effect of dry friction. The dry friction coefficient decreases with angular velocity from its static value and asymptotically approaches a constant kinetic value at infinite angular velocity. There was a good agreement of the self-excited stick-slip oscillations with field measurements.

Brett [4] showed that polycrystalline diamond compact (PDC) bits can cause severe torsional vibration, a rotary speed increase leads to a decrease in torque and higher WOB may result in severe torsional vibrations.

The torsional drillstring model proposed by Cull and Tucker [5] includes two representations for Coulomb friction: i) a piecewise friction profile and ii) a continuous and smooth nonlinear friction profile.

Mihajlović et al. [6] utilized a Coulomb friction model for the top drive and a humped friction model for the BHA and drill bit. Simulation results showed good agreement with those obtained from an experimental DS set-up.

Navarro-López and Cortés [7] used a lumped-parameter torsional model to study stick-slip oscillations. Their model includes four elements: top drive, drill pipes, BHA and the drill bit. Hopf bifurcations plots were utilized to extract the parameters that yield non-desired torsional oscillations.

Jansen [8] developed a 2 degree of freedom, rotordynamic "Jeffcott Rotor" model for a drill collar section between two stabilizers, the later modeled as bearings. Their results showed the effects of drilling fluid, stabilizer clearance and stabilizer-borehole friction on whirl amplitude, critical speed and stability. Simulation results agreed with field measurements.

Van der Heijden [9] utilized the 2 degree of freedom model of Jansen [8] to analyze the responses for chaos Poincare diagrams and Lyapunov exponents.

Kotsonis and Spanos [10] studied lateral vibrations of the BHA. The effects of fluid damping, wall contact, mass eccentricity, initial curvature of the drill collar and also linear and parametric coupling between the axial force and lateral vibration were considered. Coupling of the axial force and lateral vibrations resulted in chaotic motion. The minimum phase-volume deconvolution technique was used to identify chaos.

Yigit and Christoforou [11] utilized a lumped parameter model to investigate coupled torsional - lateral vibrations. The predicted stick-slip results were in close qualitative agreement with field measurements. An active controller mitigated stick-slip oscillations in their simulations.

Leine et al. [12] studied drillstring vibrations using sub-system models for the stick-slip and for the whirl motions. Their work showed that increasing the rotary speed will result in a change from stick-slip to whirl motion as evidenced by downhole measurements. However there was no clear evidence that decreasing the rotary speed would result in a reversal of the motion from whirl to stick-slip motion. This behavior was explained by the presence of multiple stable solutions on the bifurcation diagrams.

Yigit and Christoforou [13] employed an Euler-Bernoulli beam, assumed modes model to study the coupling of axial and lateral vibrations. The impact of the drillstring with the borehole wall was modeled using Hertzian contact theory. The coupling of the vibrations yielded a value of the critical axial load lower than the one obtained from a linear analysis and resulted in chaotic response.

Richard et al. [14] studied the coupling between the torsional and axial vibrations modes resulting from the bit-rock interaction. Their model considered the inertial moment of the BHA and showed the existence of self-excited vibrations characterized by stick-slip oscillations. It was shown that the fundamental source of the self excitation (instability) was that the cutting force and torque lagged the penetration rate.

Their work was extended by Zamanian et al. [15] who took into account the rotation of the rotary table, active damping at the top and damping of the drilling mud. Unlike the Richard et al. conclusions, they indicated that the system could always be stable by an appropriate selection of system parameters, and showed that stick-slip vibrations could be observed from the amplitude of the oscillations of the rotary table.

Yigit and Christoforou [16] investigated the coupled torsional and axial vibrations at the drill bit considering effects of weight-on-bit, torque-on-bit and cutting condition. They showed that feedback control could suppress stick-slip and bit-bounce vibrations.

Elsayed et al. [17] investigated the effect of torsion on the stability of the drillstring and on the axial and torsional loads. A lump-

parameter model was used and a mode summation method was applied to reduce the order of the system.

Christoforou and Yigit [18] studied the coupling of axial, lateral and torsional vibrations using a lumped parameter model. The coupling arose from bit-formation and drillstring-borehole interactions as well as from geometric and dynamic nonlinearities. The stick-slip and bit-bounce simulations agreed well with field observations. In addition, they designed an active controller which was effective in reducing these oscillations.

Melakhessou et al. [19] studied the contact zone of the BHA and separated it into two sections: one centered on the axis of the well and one connected to the first by a flexible string. The four-degree-of-freedom model included the effects of bending and torsion, whirling motion as well as a Coulomb type friction between a tool-joint and borehole, and the drillstring and borehole. Simulations result agreed well with those obtained with an experimental set-up and showed that their model was accurate enough to simulate the local contact between the drillstring and the borehole.

The response of drag bits (or PDC bits) was investigated by Detournay and Defourny [20]. Their model accounted for both rock cutting processes and frictional contact between the cutter wearflats and the rock. The model provided the relations between weight-on-bit, torque, angular velocity and rate of penetration.

Jogi et al. [21] determined the natural frequencies of axial, torsional and lateral vibrations of the BHA. The simulations results obtained with in-house models agreed well with field data obtained with downhole vibration measurement sensors.

Spanos et al. [22] analyzed a drillstring with a roller cone bit utilizing a finite element model. The results indicated that rotary speeds corresponding to axial natural frequencies were critical speeds causing wide fluctuation of the weight-on-bit. Increasing the rotary speed could cause the bit to lift off and the weight-on-bit to drop.

In [23], Spanos et al. employed an Euler Bernouilli, based finite element model to simulate the BHA vibrations. The effect of axial force on the lateral vibration, damping as a function of mud density and vibration frequency and the added mass of the drilling fluid were accounted for in their model.

Khulief et al. [24] modeled the drillstring including the drill pipes and drill collars using Euler-Bernoulli beam theory. Coupling of torsional and lateral inertia, axial-lateral geometric coupling, gyroscopic effect, and stick-slip interaction forces were included in the model. The effect of gravitation, generally ignored in other studies was also considered by splitting the drillstring into two sections: one in tension above the neutral point and one in compression below the neutral point. The order of the system was reduced using a modal transformation method. Transient responses resulting from various excitations were used to validate the model. Results indicated that lateral excitations affected axial and torsional vibrations and that frictional torque caused stick-slip oscillations.

The present paper extends the work of Jansen [8] and Van der Heijden [9] who analyzed the lateral vibrations of the drill collar and BHA, including stabilizers at both ends. Our contributions include modeling of drill collar flexibility utilizing finite elements and modal coordinate reduction, characterization of chaos with Lyapunov exponents and a strange attractor map, and consideration of the effects of friction, drill collar length and stabilizer gap on chaotic vibration. The upper boundary condition employed by Jansen [8] and Van der Heijden [9] is also validated by comparing responses with and without the drillpipe. A study of parameter variation for computing the Lyapunov exponents of a larger order model is included and may provide a guide for studies of chaos in other types of vibrating systems.

3 BACKGROUND THEORY

The drill collar and drillpipe shown in Figure 2 are divided into Timeshenko beam (TB) finite elements to model lateral vibrations. Let the longitudinal axis of the beam lie on the local x_1 axis. The equilibrium equations of the differential length beam subjected to shear forces V_{x_2} and bending moments M_{x_3} for the TB are given by [25] in the x_1-x_2 plane as

$$\frac{dV_{x_2}}{dx_1}=0,\ \frac{dM_{x_3}}{dx_1}+V_{x_2}=0,$$

$$M_{x_3}=EI_{x_3}\frac{d\theta_3}{dx_1},V_{x_2}=K_{S2}GA\left(-\theta_3+\frac{dv}{dx_1}\right) \tag{1}$$

where E is the modulus of elasticity, G is the shear modulus, I_{x_3} is the second moment of inertia about the x_3-axis, K_{S2} is the shear correction coefficient in x_1-x_2 plane, A is the cross-sectional area, v is the transverse deflection and θ_3 is the rotation of a transverse normal plane about the x_3-axis. The beam stiffness also includes a stress stiffening term due to gravity, F_G, acting along the axis of the drillstring. This axial tensile load increases the lateral stiffness of the drillstring and provides a pendulum restoring torque. The stress stiffening strain energy is given by [26] as

$$U_G=\frac{1}{2}\int_0^L F_G(x_1)\left\{\left(\frac{\partial u_2}{\partial x_1}\right)^2+\left(\frac{\partial u_3}{\partial x_1}\right)^2\right\}dx_1 \tag{2}$$

where u_2 and u_3 are the displacements of a point along the (x_2, x_3) coordinates. Inertia effects are modeled with a consistent mass matrix, including translational and rotary inertia terms.

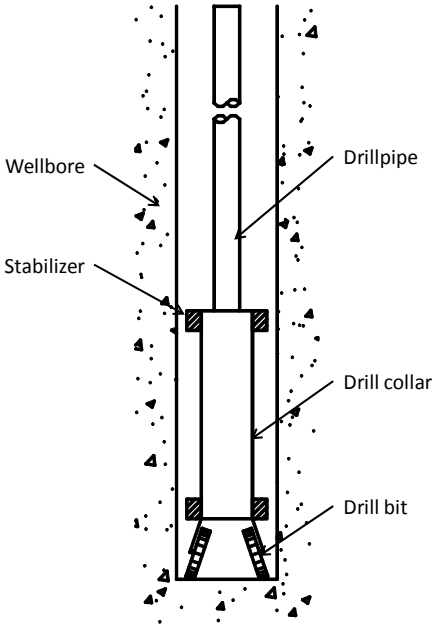

Figure 2. A General Drillstring Including the Drillpipe, Drill Collar and Drill Bit.

The imbalance forces due to mass eccentricity of the drill collar are

$$F_{e,x_2}=m_e\Omega^2e_0\cos(\Omega t),\ F_{e,x_3}=m_e\Omega^2e_0\sin(\Omega t) \tag{3}$$

where t is time, e_0 is the eccentricity of the drill collar mass (m_e) and Ω is the rotational frequency as shown in Figure 3. A nonlinear damping force due to the vibration of the drill collar in the surrounding mudflow is modeled as a velocity squared force at the midspan location on the drill collar [8, 9]:

$$F_{f,x_2} = -c_f\sqrt{\dot{x}_2^2+\dot{x}_3^2}\,\dot{x}_2,\ F_{f,x_3} = -c_f\sqrt{\dot{x}_2^2+\dot{x}_3^2}\,\dot{x}_3 \tag{4}$$

where c_f is the equivalent fluid damping coefficient. Linear damping forces are included at each stabilizer

$$F_{d,x_2} = -c_d\,\dot{x}_2,\ F_{d,x_3} = -c_d\,\dot{x}_3 \tag{5}$$

where c_d is the damping coefficient. The linear damper model is employed due to the much smaller clearance at the stabilizers (centralizers). Gyroscopic torque is neglected due to the very low speed of the drillstring.

Normal and tangential contact forces occur between the stabilizer and wellbore when the lateral displacement of the stabilizer becomes larger than the clearance, $r > s_0$ (Figure 4). The normal contact force $F_{b,r}$ is modeled as a linear spring with stiffness, k_b.

$$F_{b,r} = \begin{cases} 0 & , r < s_0 \\ k_b(r-s_0), & r > s_0 \end{cases} \tag{6}$$

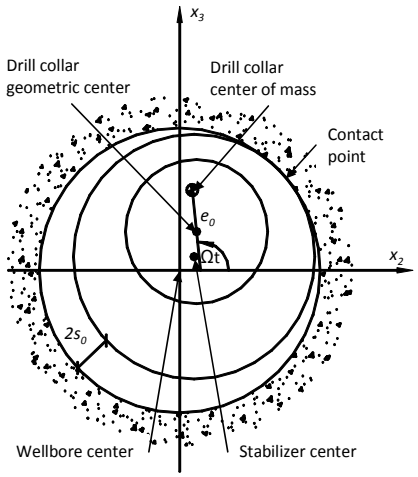

Figure 3. End View of Deflected Drill Collar Showing Mass Eccentricity and Contact Point.

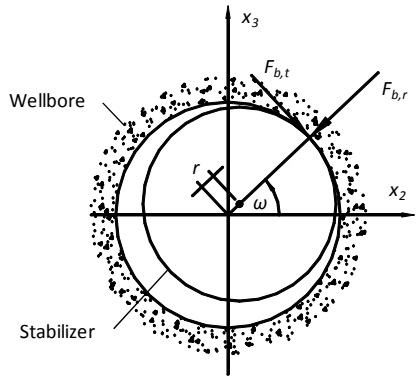

Figure 4. Contact Forces on the Stabilizer.

The tangential, coulomb friction contact force is given by

$$F_{b,t} = \mu_b\, sign(\varpi) F_{b,r} \tag{7}$$

where ω is the whirl speed and μ_b is the coefficient of friction. The stabilizer section is assumed to always slip when it contacts the wall.

The system equation of motion has the general form

$$[M]\{\ddot{q}\}+[C]\{\dot{q}\}+[K]\{q\}=\{F\} \tag{8}$$

where $\{q\}$ is the physical coordinates, $\{M\}$ is the mass matrix, $\{C\}$ is the damping matrix, $\{K\}$ is the stiffness matrix, and $\{F\}$ is the force vector including the nonlinear and imbalance forces described above. Bifurcation diagrams and Lyapunov exponents require 1000's of transient simulations. Thus the direct integration of Eq. (8) is computation time prohibitive because of the large number of degrees of freedom and the presence of nonlinear forces that require very small integration time steps. Therefore a modal condensation approach was utilized since the orthogonality conditions [27]:

$$\{\phi\}_i^T[M]\{\phi\}_i = \tilde{m}_i,\ \{\phi\}_i^T[K]\{\phi\}_i = -\tilde{m}_i\,\varpi_i^2 \tag{9}$$

yield uncoupled equations for the modal coordinates

$$\ddot{y}_i + 2\zeta_i\varpi_i\dot{y}_i + \varpi_i^2 y_i = \tilde{f}_i(t) \tag{10}$$

which are related to the physical coordinates by

$$q = \sum_{i=1}^{N_r} y_i(t)\,\phi_i \tag{11}$$

where $\{\phi\}_i$ is the mode shape, $\tilde{m}_i$ is the modal mass, ω_i is the natural frequency, ζ_i is the damping ratio, $\tilde{f}_i$ is the modal force and y_i is the modal coordinates. Equation (11) is employed to recover the physical coordinates for evaluating the nonlinear forces during the integration. The number N_r of modes retained in Eq. (11) is determined by conducting a convergence study.

Nonlinear response behavior is identified by employing one or more of the following devices: Frequency spectrums (FS), Poincaré maps (PM), Bifurcation diagrams (BD) and Lyapunov exponents (LE) [28]. The PM plots the position and velocity states at any degree of freedom for the same phase of each forcing cycle, after steady state conditions have been attained. Two dots indicate a 1/2 sub harmonic, three dots a 1/3 sub harmonic, a closed curve indicates quasi-periodic response and an area covered with points (strange attractor) indicates chaos. The BD plots the PM dots for a single state vs. a variable parameter of the system. An abrupt change in the number of dots as the parameter varies indicates the occurrence of a bifurcation such as period doubling, jump to another stable solution, etc. The LE provide a measure of the local stability of the nonlinear solution (x) by considering the convergence or divergence of linearized solutions (η) evaluated in consecutive time segments after the nonlinear solution attains steady state.

Lyapunov exponents measure divergence or convergence of trajectories near to the nonlinear system solution represented by [28]

$$\dot{x} = f(x) \tag{12}$$

The solution of the linearized form of Eq. (12) is denoted by η and obtained from

$$\dot{\eta} = A\eta \tag{13}$$

where $A = [\nabla f]$ is the $n \times n$ Jacobian matrix of f. Equations (12) and (13) are simultaneously numerically integrated after the nonlinear system has reached steady state. The linearized-system is reevaluated and integrated at equally spaced time intervals as the solution to Eq. (12) also progresses forward in time. A set of mutually orthonormal, initial condition vectors is calculated, using Gram-Schmidt orthogonalization, at the start of each time interval. Numerical integration of the linearized solution is started on each of these initial condition vectors and convergence / divergence of the resulting trajectories is evaluated. The first set of initial vectors at t_0 are:

$$\eta_1^{(0)}(t_0) = [1,0,0,...,0],\ \eta_2^{(0)}(t_0) = [0,1,0,...,0],\ \cdots,$$
$$\eta_n^{(0)}(t_0) = [0,0,0,...,1] \tag{14}$$

The Gram-Schmidt procedure is then employed to construct a new set of othonormal initial values after integrating over the interval $t_0 \le t \le t_1$. The Gram–Schmidt procedure is:

$$\eta_1^{(1)} = \eta_1^{(0)}(t_1)$$
$$\eta_2^{(1)} = \eta_2^{(0)}(t_1) - \frac{\eta_1^{(1)} \cdot \eta_2^{(0)}(t_1)}{\left\|\eta_1^{(1)}\right\|^2}\eta_1^{(1)} \tag{15}$$

through

$$\eta_n^{(1)} = \eta_n^{(0)}(t_1) - \sum_{i=1}^{n-1}\frac{\eta_i^{(1)} \cdot \eta_m^{(0)}(t_1)}{\left\|\eta_i^{(1)}\right\|^2}\eta_i^{(1)} \tag{16}$$

where $(x \cdot y)$ denotes the inner product of the vectors x and y. The set of vectors $\{\eta_1^{(1)}, \eta_2^{(1)}, ..., \eta_n^{(1)}\}$ is orthogonal, and their orthonormal forms are given by

$$\hat{\eta}_1^{(1)} = \frac{\eta_1^{(1)}}{\left\|\eta_1^{(1)}\right\|},\ \hat{\eta}_2^{(1)} = \frac{\eta_2^{(1)}}{\left\|\eta_2^{(1)}\right\|}, \cdots ,\hat{\eta}_n^{(1)} = \frac{\eta_n^{(1)}}{\left\|\eta_n^{(1)}\right\|} \tag{17}$$

The norms in the denominator of Eq. (17) are denoted by N_i^k, where the superscript refers to the *k*th time interval and the subscript refers to the *j*th vector. The Lyapunov exponents are obtained after *N* time intervals from

$$\lambda_i^{(N)} = \frac{1}{t_N - t_0}\sum_{k=1}^{N}\ln(N_i^k) \tag{18}$$

The norm N_i^k is the distance between the vectors $x(t_k) + \eta_i^{(k-1)}$ and $x(t_k)$. For a chaotic system, this distance grows nearly exponentially in time for a chaotic system so that at least one of Lyapunov exponents will become positive. The presence of chaos is indicated by a positive value of the maximum LE.

4 DRILLSTRING MODEL

4.1 Model:

The model consists of a drill collar assembly (DC) and 2 stabilizers at its end points. The Bottom Hole Assembly BHA is attached to the bottom of the drill collar in an actual drillstring. The BHA is much shorter and much lighter than the DC, therefore we treat the BHA as an integral part of the DC in the model. The model parameters are listed in Table 1. The model includes nonlinear forces, an imbalance force applied at the midspan location of the DC and linear damping at the stabilizers. The DC mass is distributed uniformly along its entire length, which is an improvement over lumping the entire mass at the DC midspan as is done in reference [8, 9]. The model is assumed to have a constant rotational speed (rpm) which is valid under the assumption of uncoupled lateral and torsional motions. An imbalance force is positioned at the DC midspan in the model. The imbalance magnitude shown in Table 1 is held constant for all results provided in this paper. The model's governing differential equations were numerically integrated with a Runge-Kutta algorithm including a variable time step.

4.2 Boundary Conditions:

The boundary conditions of the drill collar–stabilizer model are free-free when the stabilizers are not in contact with the wellbore. The lowest free – free natural frequencies and mode shapes are shown in Table 2 and Figure 5 respectively. The 1st rigid body mode is for pure translation. The second rigid body mode has a slightly positive, non-zero value due to the gravity (pendulum) restoring torque (Eq. (2)) on the rotational mode. These are some of the modes utilized in the modal response simulations discussed below.

This type of boundary condition was justified in reference [8] by the assumption that the spin (imbalance force) frequency is near the lowest mode frequency of the isolated drill collar model as totally detached from the drillpipe above it. The assumption was validated in our work by simulating the model of the DC with and without the drillpipe attached. The drillpipe was cantilevered at 100 meters above the top of the DC for this study. The ratio of the DC to drill pipe area moments of inertias was approximately 50 so that the DC is much stiffer than the drillpipe which also supports ignoring the drillpipe, by analogy to the "dog (DC) wagging the tail (drillpipe)".

Table 1. List of Drillstring Model Parameters.

Drillpipe	
Drillpipe OD	0.1016 m
Drillpipe ID	0.0848 m
Drillpipe length	100 m
Modulus of elasticity	2.1×10^{11} N/m^2
Material density	7850 kg/m^3
BHA (Drill Collar)	
Drill collar OD	0.2286 m
Drill collar ID	0.0762 m
Drill collar length, *L*	23 m
Modulus of elasticity	2.1×10^{11} N/m^2
Material density	7850 kg/m^3
Stabilizer clearance, s_0	0.0254 m
Drilling mud	
Drilling mud density	1500 kg/m^3
Fluid damping coefficient, c_f	3943.35 N.s^2 /m^2
Imbalance force	
Drill collar mass, m_e	6587 kg
Mass eccentricity, e_0	0.0127 m
Contact force	
Wellbore stiffness, k_b	1x108 N/m
Friction coefficient, μ_b	0.2
Damping at stabilizers	
Damping coefficient, c_d	300 N.s /m

Figure 6 shows the displacement response at the center of the drill collar and at one of the stabilizers for the "with" and "without" drillpipe cases, at 40 rpm. The response is seen to be sinusoidal at this rpm. Figure 7 shows the same responses at 55 rpm, at which the response is chaotic. The response locations are the same as for Figure 6. These figures clearly show almost no difference with and without the drillpipe, which supports its removal from the model from all of the remaining simulations. The bottom free boundary condition on the drill collar is most appropriate with light weight on bit (WOB) operation. A lateral degree of freedom is assumed at the bit. This is a reasonable assumption because of oversize cutting (bit walk, runout, and formation swell compensation) which leaves a clearance between the bit-through diameter and the as drilled gage hole.

Table 2. Free–Free Natural Frequencies of Drill Collar - Stabilizer Model.

Mode	Natural frequencies (Hz)	Damping ratio
1	0	-
2	0.2643	0.0166
3	2.1654	0.1361
4	5.8332	0.3665
5	11.3734	0.7146

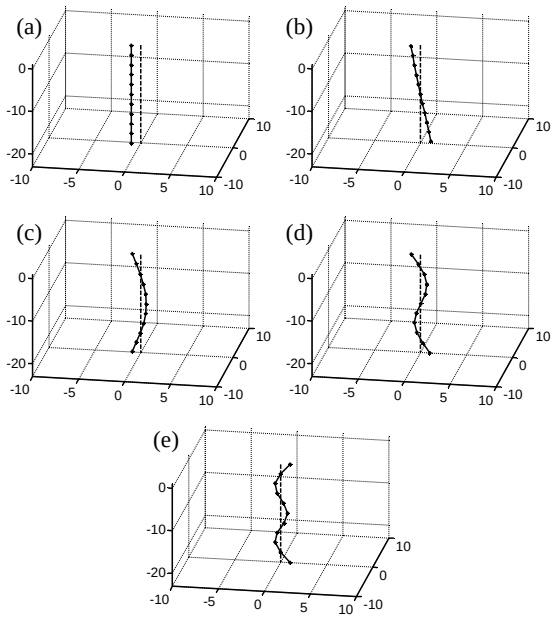

Figure 5. Lowest Mode Shapes of the Drill Collar–Stabilizer Model (a) Mode 1 (b) Mode 2 (c) Mode 3 (d) Mode 4 (e) Mode.

5 RESULTS

5.1 Nonlinear Forces:

There are 3 sources of nonlinear forces in the model, including

(a) a quadratic damper applied at the center of the drillstring to model the interaction force between the vibrating drill collar and the surrounding mud flow,

(b) the intermittent contact forces between the stabilizers and the wellbore, and

(c) the friction force between the stabilizers and the wellbore

Each of the nonlinear forces discussed above have an influence on the predicted chaotic vibrations. To illustrate this consider the next 4 figures which correspond to a model that has intermittent contact between the DC stabilizers and the wellbore wall. Figure 8(a) shows a bifurcation diagram for the model with no quadratic damping and no friction. This diagram plots the instantaneous transverse velocity at the DC midspan location at the starting time for each revolution, vs. rpm. The plot bifurcates from a sinusoidal response (single dot) to a chaotic response at 55.2 rpm. Figure 8(b) shows a bifurcation diagram for the model with quadratic damping and no friction. The plot bifurcates from a pure tone response to a chaotic response at 52.8 rpm. Figure 8(c) shows a bifurcation diagram for the model without quadratic damping and with friction. The plot bifurcates from a pure tone response to a chaotic response at 52.4 rpm. Figure 8(d) shows a bifurcation diagram for the model with quadratic damping and with friction. The plot bifurcates from a pure tone response to a chaotic response at 49.6 rpm. Clearly these figures confirm that each type of nonlinear force has an influence on the nonlinear dynamic behavior of the systems based on the changes in chaos onset speed. Figure 8(a) shows that the clearance between the wellbore and stabilizer is sufficient to cause bifurcation and chaos.

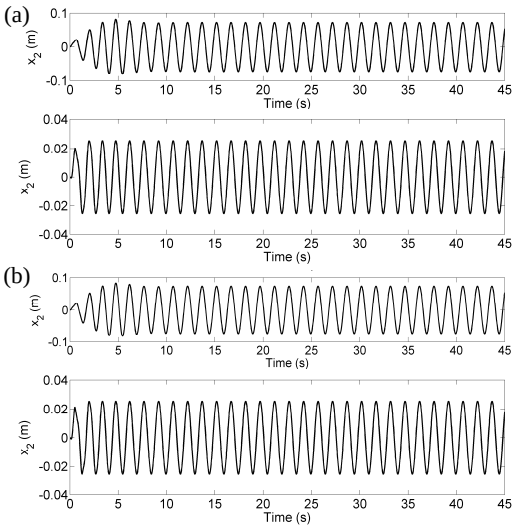

Figure 6. Vibrations at the Drill Collar Center (top) and Stabilizer (bottom), With (a) and Without (b) the Drillpipe, for a Non-Chaotic RPM.

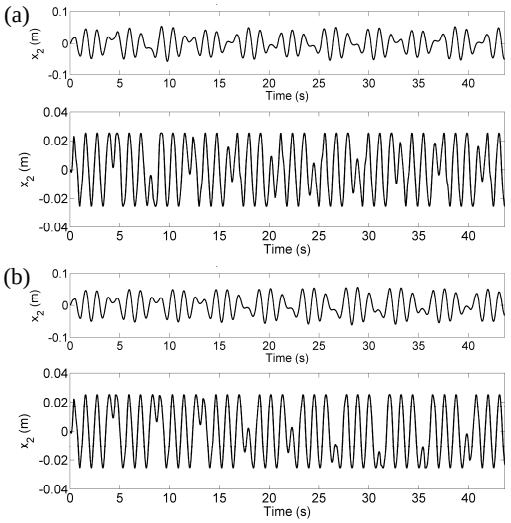

Figure 7. Vibrations at the Drill Collar Center (top) and Stabilizer (bottom), With (a) and Without (b) the Drillpipe, for a Chaotic RPM.

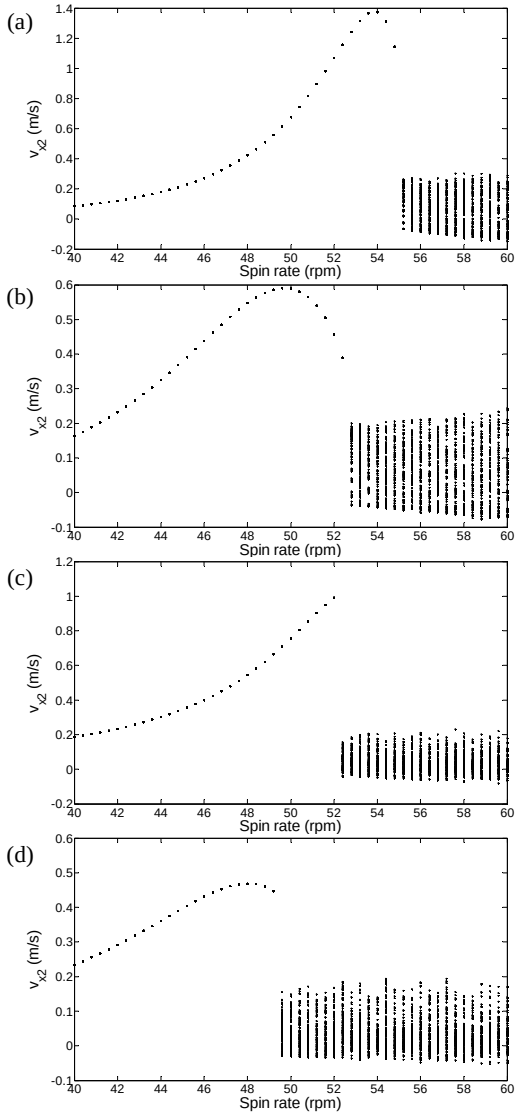

Figure 8. Bifurcation Diagrams for Model (a) without Friction and Quadratic Damping (b) without Friction and with Quadratic Damping (c) with Friction and without Quadratic Damping (d) with Friction and with Quadratic Damping.

5.2 Physical Parameter Effects:

Figure 9 shows that the chaos onset rpm and response amplitudes decrease as the coefficient of friction increases from 0.1 to 0.3. This diagram contains the transverse motion velocity at the DC midspan location. The maximum Lyapunov exponent LE was determined for the same conditions as in Figure 9 and is shown plotted against rpm in Figure 10. The zero crossings in these plots clearly confirm the transition between harmonic and chaotic response as implied in Figure 9. For sake of reference the LE's were determined after 2000 revolutions to insure steady state conditions were present prior to evaluating the LE. The number and duration of the time segments for evaluating the LE were 500 and 0.1 revolution period, respectively.

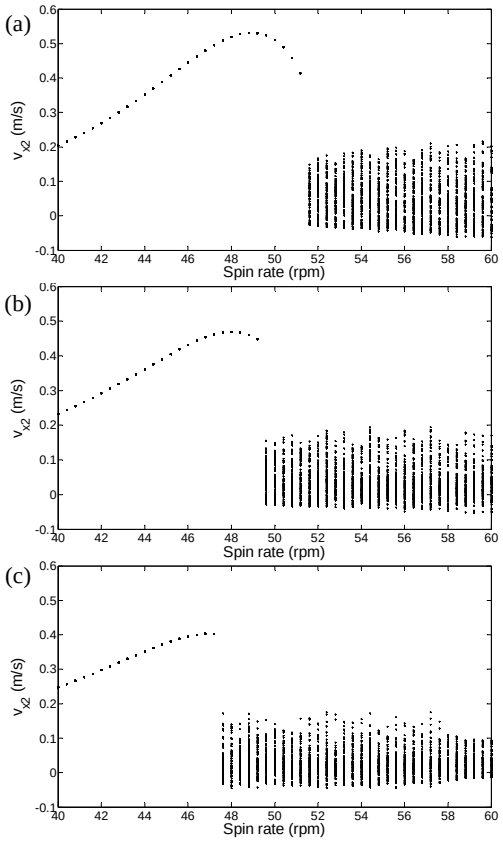

Figure 9. Bifurcation Diagrams for Model with (a) μ_b = 0.1 (b) μ_b = 0.2 (c) μ_b = 0.3.

Figure 11 shows the effect of changing the DC length on the bifurcation diagram parameters. The peak vibration amplitude and chaos onset speed are seen to decrease as the DC length increases from 15, 20, 21, 22, 23 and 25 meters.

Figure 12 shows the bifurcation diagram for the DC midspan, transverse velocity with the stabilizer radial clearance varied from 0.0127, 0.0254 and 0.0508 meters. These results indicate that clearance has a significant effect on the presence of chaos. The absence of chaos for the smallest clearance chaos indicates that a decrease in clearance may mitigate chaos.

Figure 13 shows a Poincare plot for velocity vibration at the DC midspan. Sixty thousand points are plotted forming a strange attractor for the following conditions (L = 23 m, μ_b = 0.2, 55 rpm, s_0 = 2.54 cm). This is a clear indication of chaos since the 2 dimensional, area type structure of the strange attractor is indicative of chaos whereas a closed line type structure indicates a quasi-periodic type of response.

6 CONCLUSION

The paper presented a systematic approach for predicting and analyzing the lateral vibration response of the drill collar / BHA. A lateral degree of freedom is assumed at the bit. This is a reasonable assumption because of oversize cutting (bit walk, runout, and formation swell compensation) which leaves a clearance between the bit-through diameter and the as drilled gage hole. This condition is

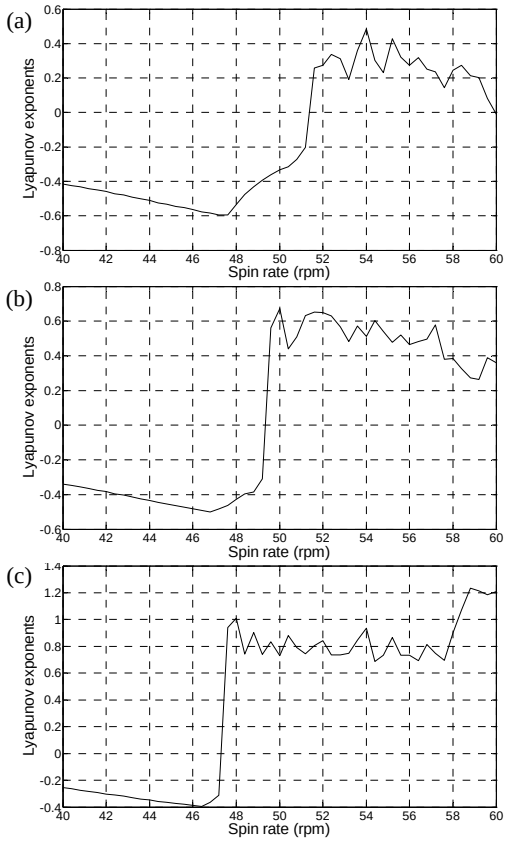

Figure 10. Maximum Lyapunov Exponent vs. Drillstring RPM with (a) μ_b = 0.1 (b) μ_b = 0.2 (c) μ_b = 0.3.

consistent with a free bottom-end boundary condition and de-coupling of the lateral vibration from the torsional and axial vibrations. Conclusions drawn from the study include:

(1) Neglect of the drillpipe at the upper boundary of the drill collar is a reasonable approximation for lateral vibration modeling of the drill collar – BHA component under rotating, light bit contact conditions.

(2) Converged Lyapunov exponents (LE) can be determined even for a system model containing many degrees of freedom such as the multi degree of freedom, modal model utilized here. The LE provided a reliable indicator of chaos as confirmed by comparison with bifurcation diagrams and Poincare (strange attractor) plots. Accurate LE's required approximately 2000 revolutions to reach steady state and approximately 500 time segments to evaluate divergence/convergence of linearized solutions, with each segment approximately 0.1revolutions in duration.

(3) Stress stiffening effects should be included in the model to account for the vertical gravity load. Thus was manifested in the non-zero rigid body pendulum mode.

(4) Gap and other nonlinear effects shift natural frequencies from their free or constrained values so that resonance peaks occur away from the linear natural frequency values.

(5) The onset speed (rpm) for chaos was shown to be significantly affected by friction, stabilizer gap and drill collar length. This onset speed was indicated by a zero crossing of the maximum Lyapunov exponent. The Lyapunov exponents were obtained via an averaging approach which depends on the length of time to steady state, the number of time segments that are utilized and the length of these time segments. Convergence studies were conducted to determine the appropriate values for these 3 factors. Figure 14(a) and (b) show how the maximum LE converges with time for both a non-chaotic and a chaotic response, respectively. The model parameters of this case are:

L =23m, μ_b = 0.1, s_0 = 2.54cm,
rpm = 50 (non-chaotic), rpm = 55 (chaotic)

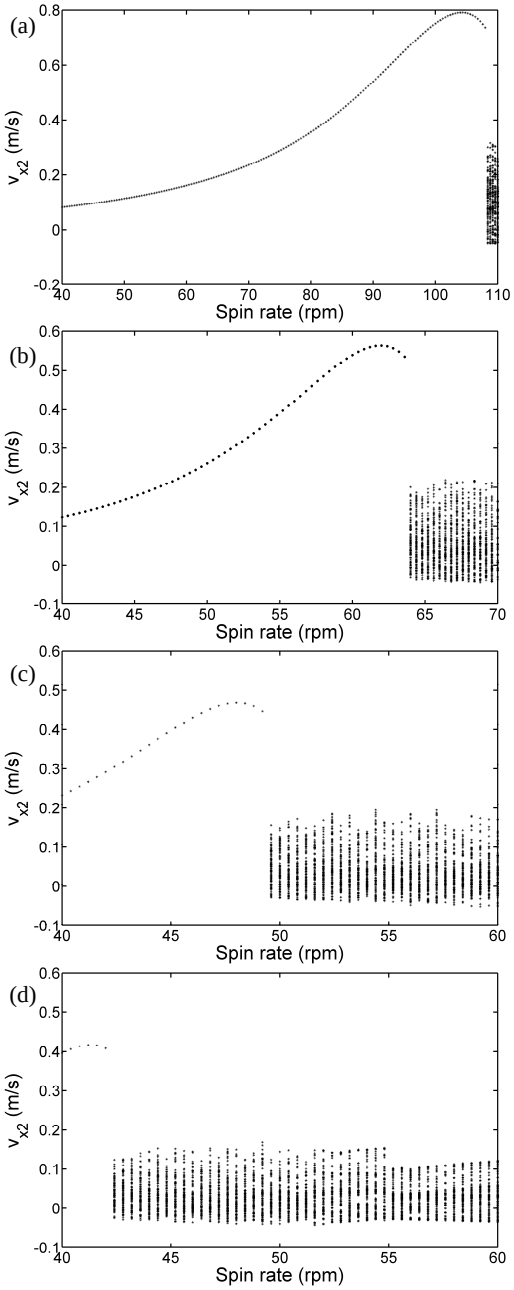

Figure 11. Bifurcation diagrams for Model with (a) 15m (b) 20m (c) 23m and (d) 25m Long Drill Collar Section.

Tables 3, 4 and 5 show the dependence and convergence properties of the LE on the 3 factors described above. Table 3 utilized 200 time segments with 0.1 revolutions per segment. Table 4 utilized 2000 revolutions as a time to steady state and 0.1 revolutions per time segment. Table 5 utilized 2000 revolutions to steady state and 500 time segments.

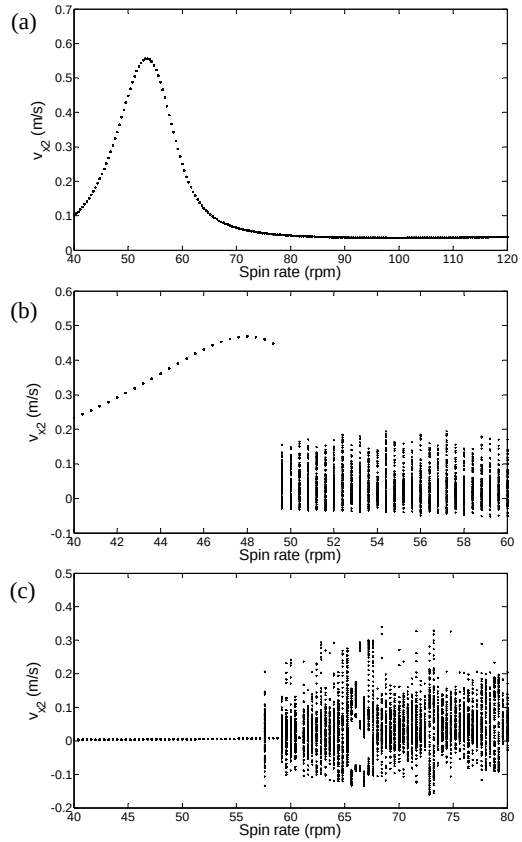

Figure 12. Bifurcation Diagram for Mid Span Transverse Velocity for Radial Clearance at Stabilizer of (a) 0.0127, (b) 0.0254 and (c) 0.0508 Meters.

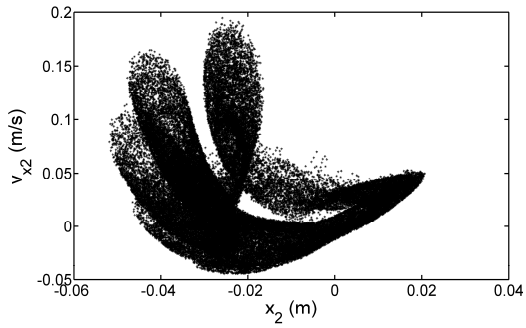

Figure 13. Poincaré Plot for Transverse Velocity at DC Midspan.

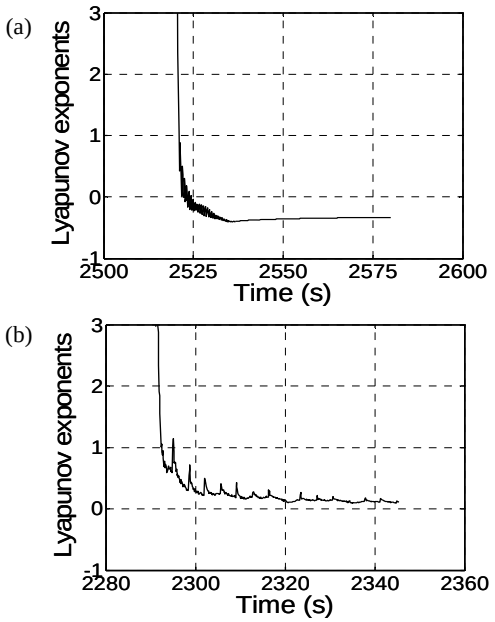

Figure 14. Maximum Lyapunov Exponent Convergence with Time for (a) a Non-Chaotic and (b) a Chaotic Response.

Table 3. Maximum Lyapunov Exponents for Different Times to Steady State.

Time to steady state (rev)	Maximum LE
50	0.3897
100	0.4714
500	0.3314
1000	0.5108
1500	0.1710
2000	0.1892
2500	0.1403
3000	0.2515
3500	0.2601
4000	0.2204
4500	0.2083
5000	0.1690

Table 4. Maximum Lyapunov Exponents Obtained from Different Numbers of Time Segments.

Number of time segments	Maximum LE
50	0.5178
100	0.2225
200	0.1892
500	0.1157
700	0.0962
1000	0.1008
1500	0.0933
2000	0.0844

Table 5. Maximum Lyapunov Exponents Obtained from Varying the Time Segment Duration.

Length of time step	Maximum LE
0.01*period	0.5178
0.05 *period	0.1746
0.10 *period	0.1157
0.20 *period	0.1005

The simulation times were considered excessive to employ physical coordinate for this study. Thus modal coordinates were employed. This required selection of the number and types of modes to utilize for convergence. Both rigid body and flexible modes were included in order to produce both types of behavior in the system response. The bifurcation diagrams were found to converge with 10 modes,

Future work will include lateral-torsional–axial coupling, the effects of PDC or roller cone bit, and drive dynamics.

7 ACKNOWLEDGEMENTS

The lead author acknowledges support from TAMU Qatar to perform the research contained in this paper.

8 REFERENCES

[1] A.T. Bourgoyne Jr., K.K. Millheim, M.E. Chenevert, F.S. Young Jr., *Applied Drilling Engineering*, Society of Petroleum Engineers, Texas, 2005.

[2] H. Rabia, *Oilwell Drilling Engineering: Principles and Practice*, Graham & Trotman, Gaithersburg, Maryland, 1985.

[3] Y.Q. Lin, Y.H. Wang, Stick-slip vibration of drill string, *ASME Journal of Engineering for Industry* 113 (1) (1991) 38-43.

[4] J.F. Brett, The genesis of torsional drillstring vibrations, *SPE Drilling Engineering* 7 (1992) 168-174.

[5] S.J. Cull, R.W. Tucker, On the modelling of coulomb friction, *Journal of Physics A-Mathematical and General* 32 (11) (1999) 2103-2113.

[6] N. Mihajlović, A.A. Van Veggel, N. Van de Wouw, H. Nijmeijer, Analysis of friction-induced limit cycling in an experimental drill-string system, *ASME Journal of Dynamic Systems*, Measurement, and Control 126 (4) (2004) 709-720.

[7] E.M. Navarro-López, D. Cortés, Avoiding harmful oscillations in a drillstring through dynamical analysis, *Journal of Sound and Vibration* 307 (1-2) (2007) 152-171.

[8] J.D. Jansen, Non-linear rotor dynamics as applied to oilwell drillstring vibrations, *Journal of Sound and Vibration* 147 (1) (1991) 115-135.

[9] G.H.M. Van der Heijden, Bifurcation and chaos in drillstring dynamics, *Chaos, Solitions & Fractals* 3 (2) (1992) 219-247.

[10] S.J. Kotsonis, P.D. Spanos, Chaotic and random whirling motion of drillstring, *ASME Journal of Energy Resources Technology* 119 (1997) 217-222.

[11] A.S. Yigit, A.P. Christoforou, Coupled torsional and bending vibrations of actively controlled drillstrings, *Journal of Sound and Vibration*, 234 (1) (2000) 67-83.

[12] R.I. Leine, D.H. Van Campen, W.J.G. Keultjes, Stick-slip whirl interaction in drillstring dynamics, *ASME Journal of Vibration and Acoustics* 124 (2) (2002) 209-220.

[13] A.S. Yigit, A.P. Christoforou, Coupled axial and transverse vibrations of oilwell drillstrings, *Journal of Sound and Vibration* 195 (4) (1996) 617-627.

[14] T. Richard, C. Germay, E. Detournay, Self-excited stick-slip oscillations of drill bits, *Comptes Rendus Mecanique* 332(8) (2004) 619-626.

[15] M. Zamanian, S.E. Khadem, M.R. Ghazavi, Stick-slip oscillations of drag bits by considering damping of drilling mud and active damping system, *Journal of Petroleum Science and Engineering* 59 (3-4) (2007) 289-299.

[16] A.S. Yigit, A.P. Christoforou, Stick-slip and bit-bounce interaction in oil-well drillstrings, *ASME Journal of Energy Resources Technology* 128 (4) (2006) 268-274.

[17] M.A. Elsayed, D.W. Dareing, M.A. Vonderheide, Effect of torsion on stability, dynamic forces, and vibration characteristics in drillstring, *ASME Journal of Energy Resources Technology* 119 (1) (1997) 11-19.

[18] A.P. Christoforou, A.S. Yigit, Fully coupled vibrations of actively controlled drillstrings, *Journal of Sound and Vibration* 267 (5) (2003) 1029-1045.

[19] H. Melakhessou, A. Berlioz, G. Ferraris, A nonlinear well-drillstring interaction model, *ASME Journal of Vibration and Acoustics* 125 (1) (2003) 46-52.

[20] E. Detournay, P. Defourny, A phenomenological model for the drilling action of drag bits, *International Journal of Rock Mechanics and Mining Sciences & Geomechanics Abstracts* 29 (1) (1992) 13-23.

[21] P.N. Jogi, Macpherson, J.D., Neubert, M., Field verification of model-derived natural frequencies of a drill string, *ASME Journal of Energy Resources Technology* 124 (3) (2002) 154-162.

[22] P.D. Spanos, A.K. Sengupta, R.A. Cunningham, Paslay, P.R., Modeling of roller cone bit lift-off dynamics in rotary drilling, *ASME Journal of Energy Resources Technology* 117 (3) (1995) 197-207.

[23] P.D. Spanos, M.L. Payne, C.K. Secora, Bottom hole assembly modeling and dynamics response determination, *ASME Journal of Energy Resources Technology* 119 (3) (1997) 153-158.

[24] Y.A. Khulief, F.A. Al-Sulaiman, S. Bashmal, Vibration analysis of drillstrings with self-excited stick-slip oscillations, *Journal of Sound and Vibration* 299 (3) (2007) 540-558.

[25] J.N. Reddy, *An Introduction to the Finite Element Method*, McGraw-Hill Higher Education, New York, 2006.

[26] R.D. Cook, D.S. Malkus, M.E. Plesha, R.J. Witt, *Concepts and Applications of Finite Element Analysis*, John Wiley & Sons, New York, 2002.

[27] W.T. Thomson, M.D. Dahleh, *Theory of Vibration with Applications*, Prentice Hall, New Jersey, 1998.

[28] D.W. Jordan, P. Smith, *Nonlinear Ordinary Differential Equations an Introduction to Dynamical Systems*, Oxford University Press, New York, 2007.